Available online at www.sciencedirect.com
SCIENCE DIRECT®
Journal of Sound and Vibration 276 (2004) 215–225
JOURNAL OF SOUND AND VIBRATION
www.elsevier.com/locate/jsvi

Bifurcation analysis of a non-linear hysteretic oscillator under harmonic excitation

Seo Il Chang*

Department of Environmental Engineering, The University of Seoul, Seoul 130-743, South Korea

Received 2 October 2002; accepted 31 July 2003

Abstract

The steady state oscillations of a system incorporating a non-linear hysteretic damper are studied analytically by applying a perturbation technique. The hysteretic damper of the system subject to harmonic resonant force is modelled by combining a Maxwell's model and Kelvin–Voigt's model in series. The non-linearity is imposed by replacing a spring element by a cubic-non-linear spring. The response of the system is described by two coupled second order differential equations including a non-linear constitutive equation. Proper rescaling of the variables and parameters of the equations of motion leads to a set of weakly non-linear equations of motion to which the method of averaging is applied. The bifurcation analysis of the reduced four-dimensional amplitude- and phase-equations of motion shows typical non-linear behaviors including saddle-node and Hopf bifurcations and separate solution branch. By the stability analysis, the saddle-node and Hopf bifurcation sets are obtained in parameter spaces. The software package AUTO is used to numerically study the bifurcation sets and limit cycle solutions bifurcating from the Hopf bifurcation points. It is shown that the limit cycle responses of the averaged system exist over broad parameter ranges.

1. Introduction

Hysteretic behavior which can be found in various elastomeric materials and civil structures has a hereditary and memory-dependent nature, which is quite often non-linear. A class of the models to describe the hysteretic cycles adopts a piecewise linear or non-linear algebraic function for force–displacement relationship. The bilinear and Ramberg–Osgood models are among them and they show the hysteretic cycles not only for the dynamic case but also for the static case. The other

*Corresponding author. Tel.: +82-2-2210-2114.
E-mail address: schang@uos.ac.kr (S. Il Chang).

0022-460X/$ - see front matter
doi:10.1016/j.jsv.2003.07.022

class of the models, so called, the differential models, accompanies constitutive differential equations and the Bouc–Wen model is one of them. Most of the models in the two classes can describe inherent non-linearities as well as the history dependency. A simpler way to produce a differential model is to combine spring and dashpot elements in various ways [1]. The Maxwell's and Kelvin–Voigt's models are the simplest among them, and the inherent non-linear property, e.g., hardening or softening stiffness, can be modelled by replacing an element by appropriate non-linear one.

When the dynamical system incorporating one of the models mentioned above is subject to harmonic forcing, the response can be obtained by solving the equations of motion and, simultaneously, the constitutive equations. Its time and frequency responses have been usually obtained by applying direct-time integration and harmonic balance methods [2], respectively, to the set of equations. The harmonic balance method has been used as a practical tool to obtain the frequency response and its stability has been determined by applying Floquet theory or Poincaré mapping [3]. Several studies [4–6] have shown that the hysteretic dynamical system can show typical non-linear behaviors which include jump, sub- and super-harmonic responses, and Hopf bifurcation [3]. The multi-valued responses and unbounded resonances have been shown to exist inherently.

Cappechi and Vestroni [4] applied the harmonic balance method to study a class of simple oscillator which has multi-linear hysteretic force–displacement relationship and it was shown that the jump phenomena can occur in the hysteretic systems. The stability analysis was performed by using the two-dimensional autonomous differential system which resulted from the harmonic balance procedure and the eigenvalues of the Jacobian matrix of the system determines the stability. The set for the vertical tangencies, i.e., the saddle-node bifurcation set and the Hopf bifurcation set of the frequency response were obtained in the parameter plane of the amplitude and frequency of excitation. In Ref. [5], the periodic responses of a differential hysteretic system were determined through the harmonic balance method with many higher order harmonic components. The stability of the periodic responses was studied by using the Poincaré mapping and it was found that in a class of oscillators saddle-node and Hopf bifurcations can occur, but no bifurcation set was given due to the limitation of the numerical method. It was shown that the super-harmonic resonances are evident in some cases. In Ref. [6], numerical multi-harmonic balance method, so called, Galerkin/Levenberg–Marquardt method was applied to Bouc–Wen differential hysteretic system, whose harmonic, sub- and super-harmonic responses were computed. It was shown that the responses can be multi-valued both in softening and hardening cases, but the stability analysis was not given. The multi-harmonic balance method combined with a path-following technique was applied to a hysteretic two-degree-of-freedom system which is in one-to-three internal resonance [11–13]. It was found that in general the frequency response curves of coupled modes exhibit various non-linear phenomena such as saddle-node bifurcation, period doubling, and sub- and super-harmonic responses. In Ref. [14], non-linear dynamic response of a self-excited non-smooth hysteretic system subject to direct excitation was studied by the method of averaging. Saddle-node and Hopf bifurcations were shown to occur and their stability boundaries were presented in the bifurcation diagrams.

The aim of this paper is to explore more rigorously the matters related with the non-linear hysteretic behaviors by applying a perturbation technique to obtain the frequency response curve and its stability and bifurcation analysis, which the previous works could not perform completely

due to the complexities of the model and the limitations of the numerical methods. For the purpose, a simple differential hysteretic oscillator which has non-linear, but continuous and smooth load–unload path is considered with direct harmonic excitation. The dynamical system incorporates a non-linear version of Burgers' model [1] which comprises of the Maxwell's and Kelvin–Voigt's in series. The response is described by the displacement equation of motion and the accompanying constitutive force equation. Applying the method of averaging [3] to the coupled second order differential equations leads to the reduced four-dimensional amplitude and phase equations of motion. The frequency response curve of the primary resonance is obtained analytically and its bifurcation is studied. The stability is determined by analyzing the singular points of the autonomous four-dimensional system and the saddle-node and Hopf bifurcation sets are obtained analytically. The limit cycle solutions bifurcating from the Hopf bifurcation points are obtained numerically by the software package AUTO [7].

2. Formulation of the problem

In this section, a set of the equations of motion of a simple mechanical system incorporating Burgers' model as a damper is derived. More detailed derivation and general result can be found in Ref. [8]. The derived equations of motion are non-dimensionalized and through proper rescalings the non-dimensional equations of motion are expressed in appropriate form for the perturbation analysis of a primary resonant response. Fig. 1 shows Burgers' four element model, which has a non-linear spring, S_1, as an element. Other elements, K_2, C_2 and C_3 are assumed to be linear. The Burgers' model has been selected to get more flexibility in modelling a hysteretic behavior and to get two-dimensional constitutive equation which is more appropriate in applying the method averaging in the perturbation analysis.

When the model is subject to a force $\hat{D}$, the non-linear spring, S_1, the Kelvin chain comprising of K_2 and C_2, and the dashpot, C_3, undergo deformations, $\hat{x}_1$, $\hat{x}_2$, and $\hat{x}_3$, respectively. The non-linearities of the spring, S_1, is assumed to be cubic as follows:

$$\hat{x}_1 = f(\hat{D}) = d_1\hat{D} + d_3\hat{D}^3, \tag{1}$$

where, in order to obtain a constitutive equation easily, the deformation $\hat{x}_1$ is described as a non-linear function of the force $\hat{D}$ instead of the force as a function of a deformation. The system parameters d_1, d_3, K_2, C_2 and C_3 can be determined through an optimization procedure for a specific damper [8]. The behaviors of the Kelvin chain and dashpot C_3 are described by the

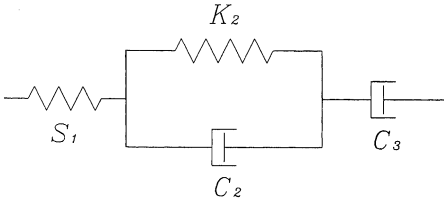

Fig. 1. Four-parameter non-linear hysteretic damper model with a non-linear spring S_1.

following equations, respectively:

$$K_2\hat{x}_2 + C_2\dot{\hat{x}}_2 = \hat{D} \tag{2}$$

and

$$C_3\dot{\hat{x}}_3 = \hat{D}, \tag{3}$$

where the dot $(\cdot)$ represents differentiation with respect to time, t. From Eqs. (1)–(3), the constitutive differential equation can be obtained as follows:

$$C_3K_2\dot{\hat{x}} + C_2C_3\ddot{\hat{x}} = C_3K_2\dot{\hat{D}}\frac{\mathrm{d}f(\hat{D})}{\mathrm{d}\hat{D}} + C_2C_3\left(\frac{\mathrm{d}f(\hat{D})}{\mathrm{d}\hat{D}}\ddot{\hat{D}} + \frac{\mathrm{d}^2f(\hat{D})}{\mathrm{d}\hat{D}^2}\dot{\hat{D}}^2\right) + K_2\hat{D} + (C_2 + C_3)\dot{\hat{D}}, \tag{4}$$

where $\hat{x} = \hat{x}_1 + \hat{x}_2 + \hat{x}_3$, which is the total deformation of the damper. The dynamic force–displacement hysteresis curves can be obtained from Eq. (4) by applying harmonic displacement, $\hat{x} = \hat{x}_0\cos(\omega t)$. Similar hysteresis curves can be obtained from Eq. (4) by applying harmonic forces. The hysteresis curves of a linear viscoelastic damper are ellipses, but due to the non-linearity in Eq. (1) the shapes of the hysteresis curves change with both dynamic amplitude and static preload. Fig. 2 shows the representative hysteresis curves of different amplitudes at zero static preload. In Fig. 2, it is shown that excessive dynamic amplitudes induce non-linear softening behaviors in the force–displacement curves.

Fig. 3 shows a schematic diagram of a spring–mass–damper system, which incorporates the non-linear hysteretic damper discussed above. The equation of motion is obtained as follows:

$$M\ddot{\hat{x}} + K\hat{x} + \hat{D} = P(t), \tag{5}$$

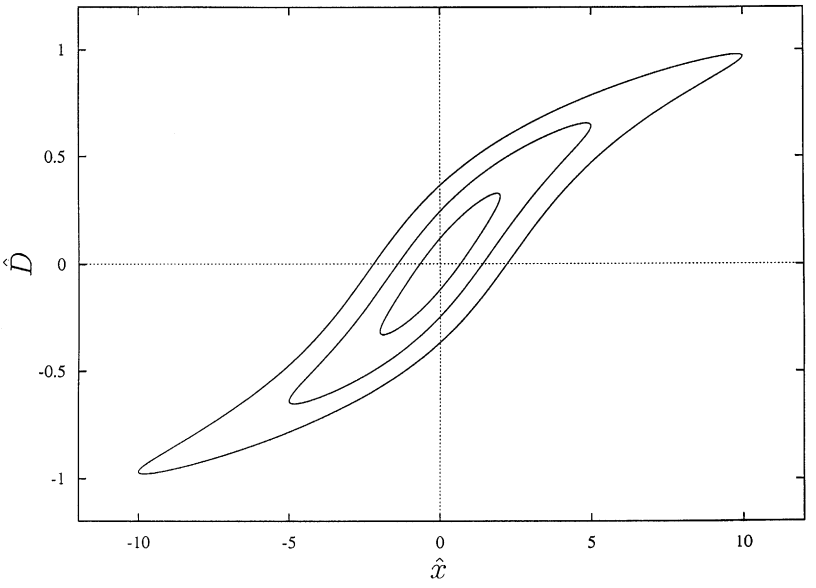

Fig. 2. Hysteresis cycles of the damper in Fig. 1; $K_2 = C_2 = C_3 = 1.0$, $d_1 = d_3 = 1.0$ in Eq. (1), $\omega = 5.0$ and $\hat{x}_0 = 2.0$ (innermost), 5.0 and 10.0.

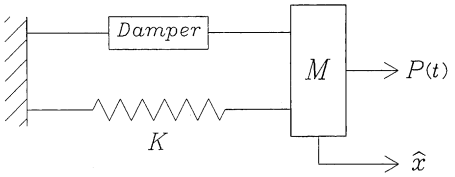

Fig. 3. Dynamic oscillator with the non-linear hysteretic damper.

where M, K and $P(t)$ are the mass, the system stiffness constant and the external excitation, respectively. The dynamics of the system is determined by the two coupled second order differential equations (4) and (5). When the system is subject to a harmonic excitation force, i.e., $P(t) = P_0 \cos(\omega t)$, the non-dimensional versions of Eqs. (4) and (5) are, respectively, as follows:

$$(1 + \bar{a}_2\bar{D}^2)\bar{D}'' + \Omega_D^2\bar{D} + \bar{a}_1\bar{D}' + 2\bar{a}_2\bar{D}\bar{D}'^2 + \frac{\bar{a}_2\bar{b}_2}{\bar{b}_1}\bar{D}'\bar{D}^2 = \bar{b}_1\bar{x}'' + \bar{b}_2\bar{x}' \tag{6}$$

and

$$\bar{x}'' + \Omega_0^2\bar{x} + \bar{C}\bar{D} = \bar{F}_0 \cos\tau, \tag{7}$$

where

$$\begin{aligned}
&\bar{x} = \frac{\hat{x}}{x_Y}, \quad \bar{D} = \frac{\hat{D}}{D_Y}, \quad \Omega_D = \frac{1}{\omega}\sqrt{\frac{K_2}{C_2C_3d_1}},\\
&\bar{a}_1 = \frac{C_2 + C_3 + C_3K_2d_1}{\omega C_2C_3d_1}, \quad \bar{a}_2 = \frac{3d_3D_Y^2}{d_1}, \quad \bar{b}_1 = \frac{x_Y}{d_1D_Y}, \quad \bar{b}_2 = \frac{K_2x_Y}{\omega C_2d_1D_Y},\\
&\Omega_0 = \frac{\omega_0}{\omega}, \quad \omega_0 = \sqrt{\frac{K}{M}}, \quad \bar{C} = \frac{D_Y}{\omega^2Mx_Y}, \quad \bar{F}_0 = \frac{P_0}{\omega^2Mx_Y}, \quad \tau = \omega t
\end{aligned} \tag{8}$$

and x_Y and D_Y represent the displacement and damper force at yielding, respectively. The primes ($'$) in Eqs. (6) and (7) represent the differentiations with respect to τ. It is assumed that primary resonant responses in the displacement $\bar{x}$ and damper force $\bar{D}$ are induced by the excitation force and that their periods are close to that of the excitation force. Such proximities of the periods can be formulated via

$$\Omega_0^2 = 1 - \varepsilon\sigma \quad \text{and} \quad \Omega_D^2 = \Omega_0^2 - \varepsilon\gamma, \tag{9}$$

where σ and γ are frequency detuning parameters between $\bar{x}$ and the excitation force, and between $\bar{x}$ and $\bar{D}$, respectively. Rescaling the variables and parameters in Eqs. (6) and (7) with the small parameter, ε, as follows:

$$\begin{aligned}
&\bar{x} = \varepsilon^{1/2}x, \quad \bar{D} = \varepsilon^{1/2}D, \quad \bar{F}_0 = \varepsilon^{3/2}F_0, \quad \bar{C} = \varepsilon C,\\
&\bar{a}_1 = \varepsilon a_1, \quad \bar{a}_2 = a_2, \quad \bar{b}_1 = \varepsilon b_1, \quad \bar{b}_2 = \varepsilon b_2,
\end{aligned} \tag{10}$$

imposing the resonance conditions in Eq. (9) and performing some algebra to uncouple the equations in inertia terms lead to

$$D'' + D + \varepsilon\left[-(\sigma + \gamma)D - a_2D^3 + a_1D' + 2a_2DD'^2 + \frac{a_2b_2}{b_1}D'D^2 + b_1x - b_2x'\right] + O(\varepsilon^2) = 0 \tag{11}$$

and

$$x'' + x + \varepsilon[-\sigma x + CD - F_0 \cos\tau] + O(\varepsilon^2) = 0. \tag{12}$$

The set of the coupled equations (11) and (12) constitutes a weakly non-linear system and the method of averaging is readily applicable to its standard form via van der Pol transformation.

3. Analysis and results

Applying the method of averaging to Eqs. (11) and (12) leads to the autonomous amplitude equations of motion, valid on a time scale $\tau \sim 1/\varepsilon$, as follows:

$$\begin{aligned}
\dot{X}_1 &= -\tfrac{1}{2}\sigma Y_1 + \tfrac{1}{2}C Y_2,\\
\dot{Y}_1 &= \tfrac{1}{2}\sigma X_1 - \tfrac{1}{2}C X_2 + \tfrac{1}{2}F_0,\\
\dot{X}_2 &= \tfrac{1}{2}b_2 X_1 + \tfrac{1}{2}b_1 Y_1 - \tfrac{1}{2}a_1 X_2 - \tfrac{1}{2}(\sigma+\gamma) Y_2\\
&\quad - \tfrac{1}{8}\frac{a_2 b_2}{b_1} X_2^3 - \tfrac{1}{8}a_2 Y_2^3 - \tfrac{1}{8}\frac{a_2 b_2}{b_1} X_2 Y_2^2 - \tfrac{1}{8}a_2 X_2^2 Y_2,\\
\dot{Y}_2 &= -\tfrac{1}{2}b_1 X_1 + \tfrac{1}{2}b_2 Y_1 + \tfrac{1}{2}(\sigma+\gamma) X_2 - \tfrac{1}{2}a_1 Y_2\\
&\quad + \tfrac{1}{8}a_2 X_2^3 - \tfrac{1}{8}\frac{a_2 b_2}{b_1} Y_2^3 + \tfrac{1}{8}a_2 X_2 Y_2^2 - \tfrac{1}{8}\frac{a_2 b_2}{b_1} X_2^2 Y_2,
\end{aligned} \tag{13}$$

where X_1 and Y_1, and X_2 and Y_2 determine the amplitudes and phases of the responses x and D, respectively, as follows:

$$x = X_1 \cos\tau + Y_1 \sin\tau \quad \text{and} \quad D = X_2 \cos\tau + Y_2 \sin\tau \tag{14}$$

and the dots $(\cdot)$ in Eq. (13) represent the differentiations with respect to slow time $\varepsilon\tau$. Via following transformation:

$$\begin{aligned}
X_1 &= R_x \cos(\phi_x), \quad Y_1 = R_x \sin(\phi_x),\\
X_2 &= R_D \cos(\phi_D), \quad Y_2 = R_D \sin(\phi_D),
\end{aligned} \tag{15}$$

Eq. (13) are written as follows:

$$\begin{aligned}
\dot{R}_x &= \tfrac{1}{2}C R_D \sin(\phi_D - \phi_x) + \tfrac{1}{2}F_0 \sin(\phi_x),\\
\dot{\phi}_x &= -\tfrac{1}{2}C\frac{R_D}{R_x}\cos(\phi_D - \phi_x) + \tfrac{1}{2}\sigma + \tfrac{1}{2}F_0\frac{1}{R_x}\cos(\phi_x),\\
\dot{R}_D &= -\tfrac{1}{2}a_1 R_D - \tfrac{1}{2}b_1 R_x \sin(\phi_D - \phi_x) + \tfrac{1}{2}b_2 R_x \cos(\phi_D - \phi_x) - \tfrac{1}{8}\frac{a_2 b_2}{b_1} R_D^3,\\
\dot{\phi}_D &= \tfrac{1}{2}(\sigma+\gamma) - \tfrac{1}{2}b_1\frac{R_x}{R_D}\cos(\phi_D - \phi_x) - \tfrac{1}{2}b_2\frac{R_x}{R_D}\sin(\phi_D - \phi_x) + \tfrac{1}{8}a_2 R_D^2.
\end{aligned} \tag{16}$$

From Eqs. (16), through some algebra, it can be shown that the steady state constant solution, R_D can be obtained by solving the following equation:

$$\begin{aligned}
&a_2^2(b_1^2 + b_2^2)\sigma^2 R_D^6 + 8\sigma a_2 b_1[(b_1\delta + a_1 b_2)\sigma - C(b_1^2 + b_2^2)]R_D^4\\
&\quad + 16 b_1^2[(\delta^2 + a_1^2)\sigma^2 - 2C(b_1\delta + a_1 b_2)\sigma + C^2(b_1^2 + b_2^2)]R_D^2 - 16F_0^2 b_1^2(b_1^2 + b_2^2) = 0,
\end{aligned} \tag{17}$$

where $\delta \equiv \sigma + \gamma$ and the steady state constant solution, R_x, is described by

$$R_x^2 = \frac{R_D^2}{16b_1^2(b_1^2+b_2^2)}[a_2^2(b_1^2+b_2^2)R_D^4 + 8b_1a_2(b_1\delta + a_1b_2)R_D^2 + 16b_1^2(\delta^2+a_1^2)]. \tag{18}$$

The representative bifurcation diagrams of the response R_D with respect to the detuning parameter σ with a stability boundary [9] are shown in Fig. 4. The responses inside the stability boundary curve, named as SB in Fig. 4, are unstable. Fig. 4 shows that a separate solution branch can coexist with the primary solution branch for the cases $F_0 = 1.74$ and 1.80, and that, through merging of the two solution branches, the connected solution branches are formed for the case $F_0 = 1.88$. Even when the primary solution branch shows no apparent non-linear behavior ($F_0 = 1.74$), such as jump phenomena, the separate solution branch exists. The stability boundary of saddle-node bifurcation in Fig. 4 can be obtained by imposing the geometric vertical tangency condition $\partial\sigma/\partial R_D = 0$ to Eq. (17). The representative saddle-node bifurcation set which can be obtained by combining the vertical tangency condition and the solution of Eq. (17) is shown in Fig. 5. The saddle-node bifurcation set can explain the existence of the separate solution branch for the case $F_0 = 1.74$, the occurrences of the three saddle-node bifurcations for the case $F_0 = 1.80$ and the connected solution branches for the case $F_0 = 1.88$ in Fig. 4. For either of the cases $F_0 = 1.74$ and 1.88, there exists only one saddle-node bifurcation, but for the former case, the saddle-node bifurcation occurs in the separate solution branch and for the latter, it occurs in the connected lower solution branch. The non-linear phenomena including the jumps and merging of the primary and separate branches have been shown to exist in the dynamical systems incorporating other types of the non-linear model [4–6]. The saddle-node bifurcation set in Fig. 5 is comparable to the curves C_1 and C_2 in Fig. 10 in Ref. [4] in which a multi-linear model is considered.

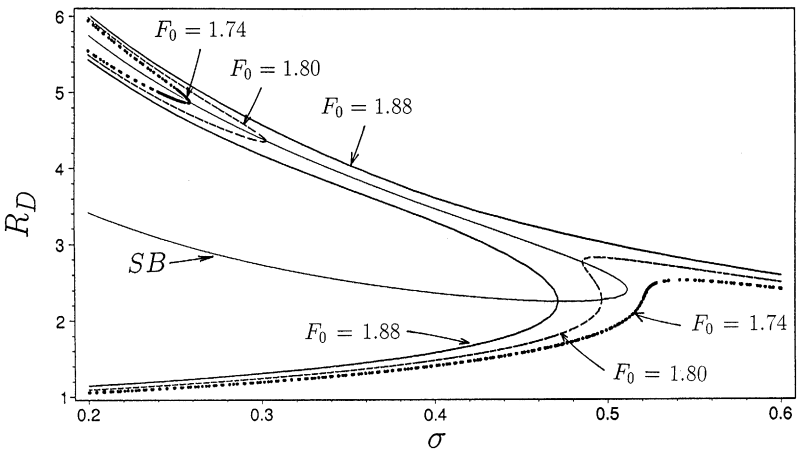

Fig. 4. Bifurcation diagrams (response R_D vs. frequency detuning parameter σ) with the stability boundary curve (SB; thin solid line) of saddle-node bifurcation; $a_1 = 3.0$, $a_2 = b_1 = b_2 = 1.0$, $C = 2.0$, $\gamma = 0.0$, $F_0 = 1.74$ (dotted line), 1.80 (dashed line) and 1.88 (solid line).

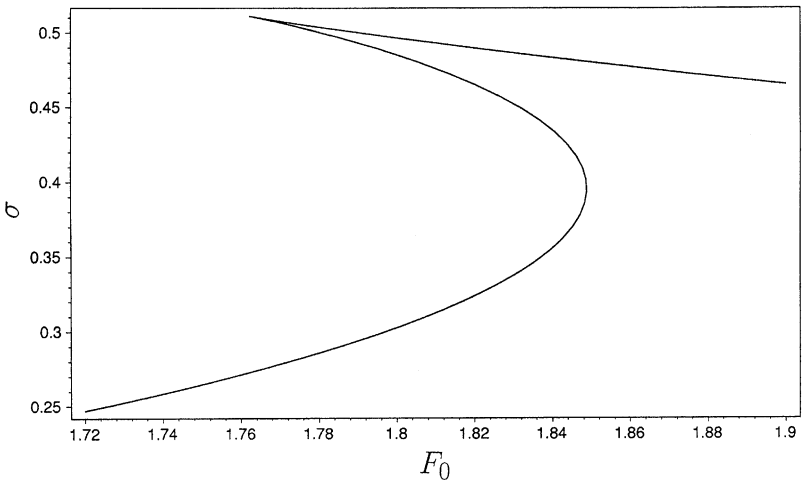

Fig. 5. Saddle-node bifurcation set in σ–F_0 plane; $a_1 = 3.0$, $a_2 = b_1 = b_2 = 1.0$, $C = 2.0$, $\gamma = 0.0$.

The stability analysis is performed by referring to the Jacobian of Eq. (13) and by denoting the eigenvalue by λ, the characteristic equation is as follows:

$$J_4\lambda^4 + J_3\lambda^3 + J_2\lambda^2 + J_1\lambda + J_0 = 0, \tag{19}$$

where the coefficients J_0, J_1, J_2, J_3 and J_4 are the functions of the system parameters and their lengthy expressions are not presented here. For stable solutions, Routh–Hurwitz criteria require that [10]

$$J_0 > 0, \quad J_1 > 0, \quad J_2 > 0, \quad J_3 > 0, \quad J_4 > 0 \tag{20}$$

and, in addition,

$$J_1(J_2J_3 - J_1J_4) - J_0J_3^2 > 0. \tag{21}$$

By numerically studying and plotting the conditions in Eq. (20), it has been found that the first condition in Eq. (20) agrees with the saddle-node bifurcation set in Fig. 5.

Another possibility losing stability is due to Hopf bifurcation [3], through which limit cycle solution bifurcates from the steady state constant solution. In Fig. 6 is shown the bifurcation diagram of the response R_D with respect to the another detuning parameter γ and the stability boundaries obtained from the first condition in Eq. (20) for the saddle-node bifurcation and from Eq. (21) for Hopf bifurcation. The thick solid and dashed lines represent the stable and unstable steady state constant solutions, respectively, and the squares represent the Hopf bifurcation points. The corresponding saddle-node bifurcation set in σ–γ plane is presented in Fig. 7. The Hopf bifurcations have been shown to exist in the dynamical systems incorporating other types of the non-linear model [4,5].

The limit cycle solutions bifurcating from the Hopf bifurcation points can be found by using AUTO [7], a numerical software package which can perform bifurcation analysis and continuation of solutions for ordinary differential equations. The representative bifurcation diagram obtained by using AUTO to Eq. (13) is presented in Fig. 8, where it is shown the limit

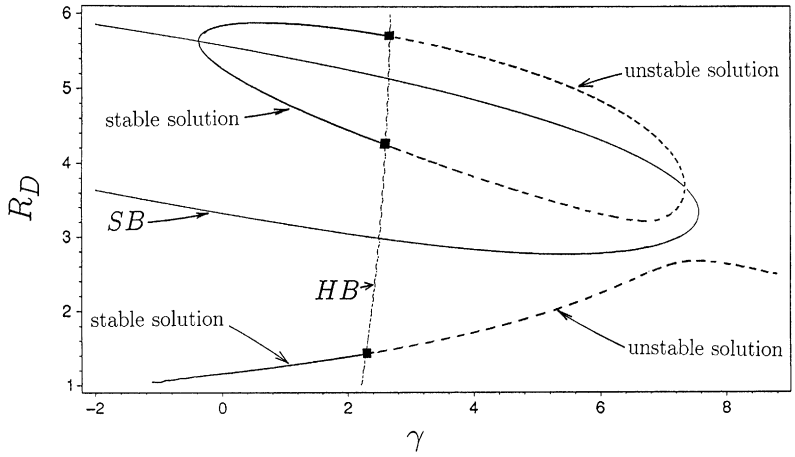

Fig. 6. Bifurcation diagram (response R_D vs. second frequency detuning parameter γ) with the stability boundaries of saddle-node (SB; thin solid line) and Hopf (HB; thin dashed line) bifurcations; $a_1 = 3.0$, $a_2 = b_1 = b_2 = 1.0$, $C = 2.0$, $\sigma = 0.21$, $F_0 = 1.88$.

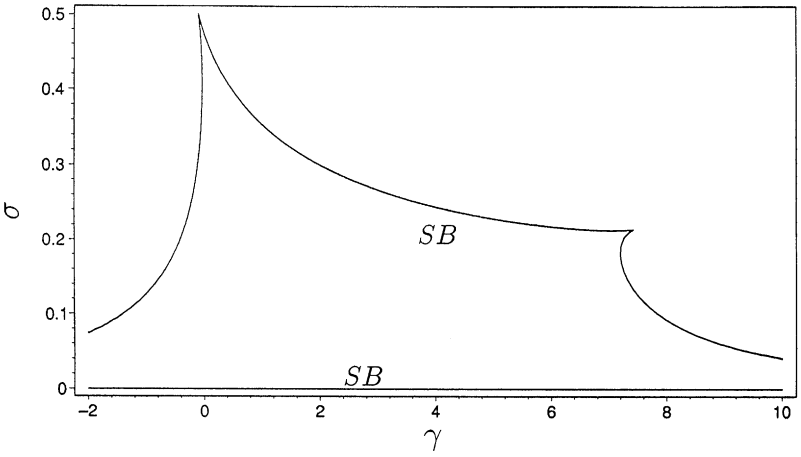

Fig. 7. Saddle-node bifurcation set in σ–γ plane; $a_1 = 3.0$, $a_2 = b_1 = b_2 = 1.0$, $C = 2.0$, $F_0 = 1.88$.

cycle solution branches are bifurcating from the steady state constant solution branches via super- and sub-critical Hopf bifurcations. The solid and open circles represent stable and unstable limit cycle solutions, respectively and the squares represent the Hopf bifurcation points. The solid and dashed lines represent the stable and unstable steady state constant solutions, respectively.

In general, the saddle-node and Hopf bifurcation sets can be obtained numerically by using AUTO, and the results have been found to be comparable numerically with those of the analytical study or Eqs. (20) and (21). The representative Hopf bifurcation set is shown in Fig. 9 together with the saddle-node bifurcation set. The bifurcation sets in Fig. 9 are the result of the analytical stability study and it is shown that the saddle-node bifurcation set meets the Hopf bifurcation set at point P, at which two Hopf bifurcation points and a saddle-node bifurcation point in the corresponding bifurcation diagram coincide.

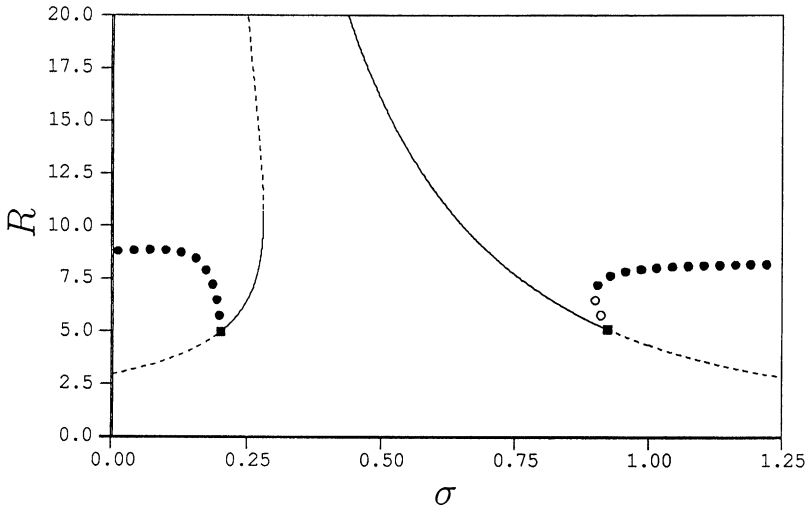

Fig. 8. Bifurcation diagram with periodic solution branches; $a_1 = 3.0$, $a_2 = b_1 = b_2 = 1.0$, $C = 2.0$, $\gamma = 2.50$, $F_0 = 1.88$, $R = \sqrt{R_x^2 + R_D^2}$ (result of numerical study).

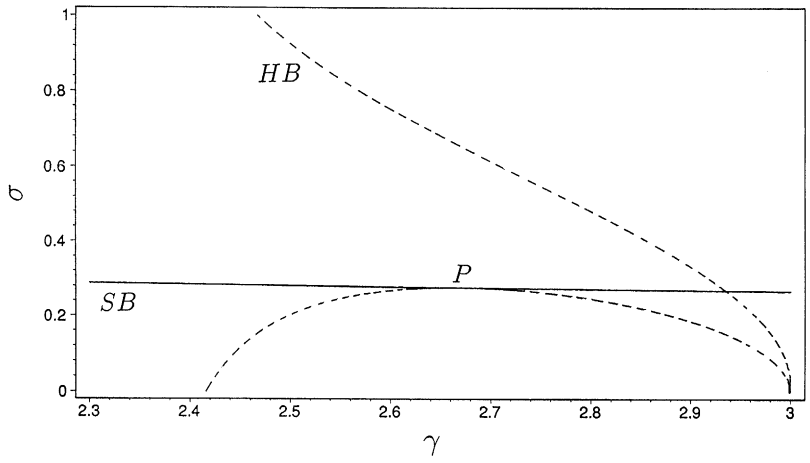

Fig. 9. Hopf (HB; dashed line) and saddle-node (SB; solid line) bifurcation sets in σ–γ plane; $a_1 = 3.0$, $a_2 = b_1 = b_2 = 1.0$, $C = 2.0$, $F_0 = 1.88$ (result of analytical study).

4. Summary and conclusions

The response of the oscillator adopting a non-linear version of Burgers' model as a hysteretic damper is governed by the two coupled second order differential equations including the non-linear constitutive equation. Applications of van der Pol transformation and the method of averaging lead to the reduced four-dimensional amplitude and phase equations from which the steady state constant and periodic responses can be obtained. The local bifurcation analysis of the reduced equations gives the bifurcation sets for the saddle-node and Hopf bifurcations. The

responses for various levels of parameter values exhibit non-linear behaviors including jump, isolated response branch and limit cycle motion of the reduced averaged system. The periodic solution branches bifurcating from the Hopf bifurcation points have been found from the numerical study.

Recently, as mentioned above, some efforts [11–13] have been spent to study the non-linear dynamics of a hysteretic two-degree-of-freedom system which is in one-to-three internal resonance. The numerical multi-harmonic balance method has been used as a useful and practical tool to obtain sub- and super-harmonic responses as well as primary resonant response. The perturbation methods including the method of averaging used in this work are expected to be an effective tool to perform bifurcation analysis of such a two-degree-of-freedom system provided a continuous and smooth hysteretic load–unload cycle is incorporated. Although complicated analysis of higher-dimensional system including constitutive equations is expected to be required, the analytical study of the two-degree-of-freedom system remains as a valuable future work provided abundant amount of algebra to reduce it to the averaged system can be managed appropriately.

Acknowledgements

The author acknowledges the valuable comments from the reviewers. This work was supported by Korea Research Foundation Grant KRF-1998-018-E00050.

References

[1] W.N. Findley, J.S. Lai, K. Onaran, *Creep and Relaxation of Nonlinear Viscoelastic Materials: with an Introduction to Linear Viscoelasticity*, Dover Publications, New York, 1989.
[2] A.H. Nayfeh, D.T. Mook, *Nonlinear Oscillations*, Wiley, New York, 1979.
[3] J. Guckenheimer, P. Holmes, *Nonlinear Oscillations, Dynamical Systems, and Bifurcations of Vector Fields*, Springer, New York, 1983.
[4] D. Capecchi, F. Vestroni, Periodic response of a class of hysteretic oscillators, *International Journal of Non-linear Mechanics* 25 (1990) 309–317.
[5] D. Capecchi, Periodic response and stability of hysteretic oscillators, *Dynamics and Stability of Systems* 6 (1991) 89–106.
[6] C.W. Wong, Y.Q. Ni, S.L. Lau, Steady-state oscillation of hysteretic differential model. I: response analysis, *Journal of Engineering Mechanics American Society of Civil Engineers* 120 (1994) 2271–2298.
[7] E. Doedel, *AUTO*: *Software for Continuation and Bifurcation Problems in Ordinary Differential Equations*, Department of Applied Mathematics, California Institute of Technology, 1986.
[8] F. Gandhi, I. Chopra, A time-domain non-linear viscoelastic damper model, *Smart Materials and Structures* 5 (1996) 517–528.
[9] D.W. Jordan, P. Smith, *Nonlinear Ordinary Differential Equations*, 2nd Edition, Clarendon Press, Oxford, 1991.
[10] P.R. Sethna, A.K. Bajaj, Bifurcations in dynamical systems with internal resonance, *Journal of Applied Mechanics American Society of Mechanical Engineers* 45 (1978) 895–902.
[11] D. Capecchi, F. Vestroni, Asymptotic response of a two DOF elastoplastic system under harmonic excitation. Internal resonance case, *Nonlinear Dynamics* 7 (1995) 317–333.
[12] D. Capecchi, R. Masiani, F. Vestroni, Periodic and non-periodic oscillatios of a class of hysteretic two degree of freedom systems, *Nonlinear Dynamics* 13 (1997) 309–325.
[13] R. Masiani, D. Capecchi, F. Vestroni, Resonant and coupled response of hysteretic two-degree-of-freedom systems using harmonic balance method, *International Journal of Non-Linear Mechanics* 37 (2002) 1421–1434.
[14] Q. Ding, A.Y.T. Leung, J.E. Cooper, Dynamic analysis of a self-excited hysteretic system, *Journal of Sound and Vibration* 245 (2001) 151–164.